Nanoscale

ROYAL SOCIETY OF CHEMISTRY

PAPER

View Article Online
View Journal | View Issue

Cite this: *Nanoscale*, 2022, **14**, 1452

SERS tags derived from silver nanoparticles and aryl diazonium salts for cell Raman imaging†

Da Li,[a] Philippe Nizard,*[a] Delphine Onidas,[a] Aazdine Lamouri,[b] Jean Pinson,[b] Samia Mahouche-Chergui,[c] Kelly Aubertin,[d] Florence Gazeau,[d] Yun Luo*[a] and Claire Mangeney*[a]

The surface functionalization of silver nanoparticles (NPs) by Raman reporters has stimulated a wide interest in recent years for the design of Surface-Enhanced Raman Spectroscopy (SERS) labels. However, silver NPs are prone to oxidation and aggregation, which strongly limits their applications. The design of stable SERS tags based on Ag NPs still represents a major challenge for Raman bioimaging. We address this issue herein by taking advantage of aryl diazonium salt chemistry to obtain stable Ag NPs functionalized by multifunctional polyaryl layers bearing different Raman reporters ($-NO_2$, $-CN$, $-CCH$). The resulting SERS-encoded Ag NPs were characterized by UV-vis absorption, transmission electron microscopy (TEM) and SERS. The formation of multilayers at the surface of Ag NPs gives access to new spectrally distinguishable SERS codes thus broadening the library of available Raman tags. Proof-of-concept Raman imaging experiments were performed on cancer cells (HeLa) after NP uptake, highlighting the large potentials of diazonium salt chemistry to design Ag NPs-based SERS labels for Raman bioimaging.

Received 16th May 2021,
Accepted 4th January 2022

DOI: 10.1039/d1nr03148a

rsc.li/nanoscale

Introduction

Sensing and imaging technologies based on the use of optically encoded particles have received growing interest these last decades for medical diagnosis and bioimaging.[1–4] Among the portfolio of reported encoded particles, optical labels based on plasmonic nanoparticles (NPs) are particularly attractive, due to their unique plasmon resonance properties resulting in enhanced electromagnetic fields at the NP surface.[5,6] This property has been exploited in Surface-Enhanced Raman Spectroscopy (SERS) to enhance the Raman scattering of molecular probes adsorbed onto metallic NPs,[7,8] yielding SERS-encoded NPs. Advantages of SERS labels over fluorescent probes include the sharp "fingerprint" signals of Raman spectra with multiple sets of narrow peaks, providing high multiplexing capacity with negligible photobleaching.[9–11] The choice of the metallic core in SERS-encoded NPs is a critical parameter.[12,13] Gold NPs are very popular because they exhibit superior biocompatibility and long-term stability. In contrast, silver NPs are easily oxidized and less stable than gold NPs. However, they are cheaper to produce and are the most efficient Raman signal-enhancing materials. Indeed, they give rise to intense SERS signals, typically 10 to 100 times higher than the ones obtained with similar gold NPs, due to lower damping rates of the plasmon mode.[14–16] The design of robust and stable SERS tags based on Ag NPs is thus a critical issue for Raman imaging. To obtain bright SERS tags with improved chemical stability and biocompatibility, various surface modification strategies of Ag NPs have been reported using thiols,[17,18] silica[19] or polymer layers.[20,21] However, thiols are prone to degradation upon laser irradiation and can be exchanged in complex biological media, compromising their efficacy and reliability.[22,23] The coating of Ag NPs by silica or polymer layers proved efficient to protect and stabilize the tags. For example, monodisperse polymer-coated Ag nanorods encoded with five different Raman reporter molecules were elaborated and evaluated for intracellular SERS imaging.[24] Thanks to the polymer coating, the nanohybrids displayed long-term stability, low cytotoxicity and high biocompatibility. However, this approach involves additional chemical layers and multistep procedures. The development of alternative surface functionalization strategies to obtain a wide range of chemically stable silver-based SERS-encoded NPs remains therefore an important challenge.

The use of surface functionalization agents based on aryl diazonium salts has been proposed recently as an alternative to thiol self-assembled monolayers for the modification of plasmonic nanoparticles.[25,26] The main interests of these

[a]*Address Université de Paris, Lab Chim & Biochim Pharmacolog & Toxicol, UMR 8601, F-75006 Paris, France. E-mail: claire.mangeney@parisdescartes.fr, philippe.nizard@parisdescartes.fr, yun.luo@parisdescartes.fr*
[b]*Université de Paris, ITODYS, UMR 7086, 75013 Paris, France*
[c]*Université Paris-Est, ICMPE, UMR7182, 94320 Thiais, France*
[d]*Université de Paris, MSC, CNRS UMR 7057, 75013 Paris, France*

†Electronic supplementary information (ESI) available. See DOI: 10.1039/d1nr03148a

molecules for surface functionalization rely on (i) the simple protocols for their synthesis and surface grafting,[27–29] (ii) the wide range of available terminal groups, (iii) the creation of strong surface-C interfacial bonds[30] and (iv) the possibility to form multifunctional polyaryl layers due to the high reactivity of aryl radicals, generated upon decomposition of the diazonium salts. Owing to these interesting properties, aryl diazonium salts were applied to the functionalization of plasmonic NPs for various applications, including bioimaging,[31] nanosensors[32,33] and antimicrobial materials.[34] Recently, these molecules were also used as Raman reporters for the design of SERS encoded gold NPs.[35] The resulting Au nanoprobes combined unique SERS spectra and post-functionalization capacity for the attachment of a nucleotide, adenosine 5′-monophosphate. This nucleotide was identified recently as a tumour-targeting ligand, through adenosine A1 receptor.[36] However, the use of diazonium salts for the elaboration of SERS tags based on silver NPs has never been reported yet.

We fill this gap in the present paper by taking advantage of the valuable features of aryl diazonium salts to design robust Ag-based SERS labels with large encoding capabilities due to the surface polymerization of various encoding elements. Spherical Ag NPs were chosen here as proof of concept as they are simple to prepare and they are used extensively in the literature. However, it is noteworthy that diazonium salt chemistry was successfully applied in the literature to plasmonic NPs with various shapes including spheres, rods,[28] triangles,[37] stripes,[29] multibranched[34] and dendrimers.[38] Therefore, this study should be easily adaptable to a wide range of plasmonic NPs, including anisotropic Ag NPs. Three aryl diazonium salts with different *para*-substituents (–NO_2, –C≡N, –C≡C–H) were selected due to their intense and characteristic SERS signals[39] making them ideal candidates to act as Raman reporters. They were used either as single functional layers around Ag NPs providing a SERS signature characteristic of the chosen functional group or as multifunctional layers, combining different SERS signatures and giving access to new spectrally distinguishable codes (see Fig. 1). The resulting SERS-encoded Ag NPs were characterized by UV-vis absorption, TEM and SERS.

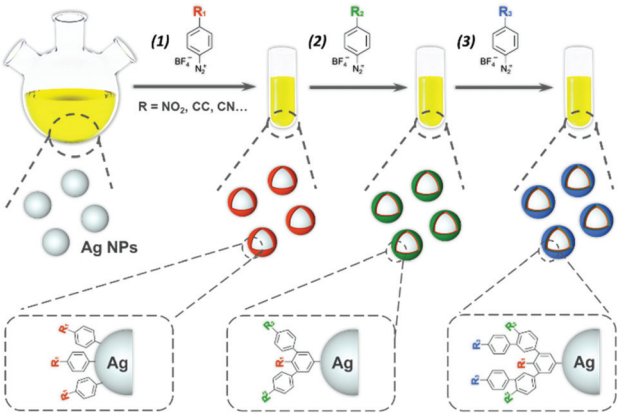

Fig. 1 Representative scheme of the preparation process of SERS encoded tags based on aryl diazonium salt chemistry. Aqueous Ag NPs solutions were mixed with aryl diazonium salts bearing different Raman reporter groups (R_{1-3} = NO_2, C≡CH, C≡N), following a sequential process.

Experimental

Synthesis of aryl diazonium salts (D-NO_2, D-CCH and D-CN)

Aryl diazonium salt D-NO_2 was prepared by the method published previously by our group.[35] 2 g of 4-nitroaniline (≥99%, Sigma-Aldrich) and 10 mL of acetonitrile (≥99.9%, Sigma-Aldrich) were sequentially added to 12 mL of tetrafluoroboric acid (48% in H_2O, Sigma-Aldrich). Then the mixed solution was transferred to an ice water bath and cooled down to 2 °C under continuous stirring. Afterwards, 2 mL of *tert*-butyl nitrite (90%, Sigma-Aldrich) was added to the reaction solution drop by drop. The solution was incubated for 30 min under stirring. After 3 times washes by diethyl ether (≥99.7%, Sigma-Aldrich), the resulting diazonium salt D-NO_2 was dissolved in acetone (≥99.9%, Sigma-Aldrich) and kept at room temperature for drying. For the preparation of D-CCH and D-CN, 4-ethynylaniline (97%, Sigma-Aldrich) and 4-aminobenzonitrile (98%, Sigma-Aldrich) were used as corresponding precursors based on the same protocol.

Synthesis of citrate-coated silver NPs

Ag NPs were synthesized by the reduction of silver nitrate (≥99.0%, Sigma-Aldrich) based on previous report.[40] Briefly, 80 μL of 0.1 M L-ascorbic acid (99%, Sigma-Aldrich) and 1.1 mL of 0.1 M sodium citrate (anhydrous, ≥99.5%, Sigma-Aldrich) were added to 80 mL boiling deionized water simultaneously. After boiling for 1 min, 2 mL of 0.01 wt% polyvinylpyrrolidone (average mol wt 360 000, Sigma-Aldrich) and 240 μL of 0.1 M aqueous silver nitrate were injected to the boiling solution under continuous stirring. The color of the solution changed from colorless to orange quickly. After 5 minutes of reaction, the heating and stirring were stopped and the solution was cooled down to room temperature.

Surface functionalization of Ag NPs by diazonium salts

For surface functionalization of Ag NPs, 10 μL of aryl diazonium salts (D-NO_2, D-CCH or D-CN, concentration of 10^{-3} M) were added into 2 mL Ag NPs solution and left to react for 60 min at room temperature. Then 40 μL of 0.01 wt% polyvinylpyrrolidone were added to the solution for stabilization of the NPs. After 60 min at room temperature, the functionalized Ag NPs were washed in deionized water with a centrifugation/redispersion process for 3 times and the obtained samples were noted Ag@R_1 (R_1 stands for the functional group of the grafted polyaryl layer). The second and third polyaryl layers were grafted with a similar functionalization process and the corresponding samples were named Ag@R_1@R_2 and Ag@R_1@R_2@R_3, respectively.

Cell culture, uptake and cytotoxicity

HeLa-HSP70/GFP cells[41] were grown in DMEM (Gibco) added by 10% FBS (Corning), 1% antibiotics (50 unitsper mL of peni-

cillin 50 μg mL^{-1} of streptomycin) (Gibco) and Geneticin (100 μg mL^{-1}) (Gibco), at 37 °C, 5% of CO_2 and 90% of humidity.

For the investigation of cell uptake, 300 000 HeLa-HSP70/GFP cells in 2 mL of medium were seeded in a 6 wells plate (each well containing a coverslip previously incubated for 5 min in ethanol 70% and rinsed 3 times with PBS 1×). After 24 hours, the medium was replaced with 2 mL of fresh medium containing diazonium modified Ag NPs. For this, the bare and functionalized NPs were previously washed in water and re-suspend with 2 mL of medium to reach a 20 μg mL^{-1} concentration. Each type of functionalized Ag NPs was incubated individually with cells. After incubating for 6 h, cells were rinsed with PBS 1× (tablet, Sigma-Aldrich) once and incubated for 30 min with 4% PFA (16%, Alfa Aesar™, FisherScientific) solution. The coverslips were ready for SERS analysis after 3 washes with deionized water. Cytotoxicity was assessed by AlamarBlue™ assay (InVitrogen). 3000 cells HeLa-HSP70 /GFP were seeded in each well of a 96-wells plate in 200 μL of medium. After 24 hours, medium was replaced by 200 μl of medium containing diazonium modified Ag NPs and cells were incubated for further 6 hours. Then medium was replaced by 100 μL of medium containing 10% of AlamarBlue™ and incubated for 18 h. Then the fluorescence (Ex 540–Em 590) associated to the wells were read on a SpectraMax® iD3Multi-Mode Microplate Reader (Molecular Devices). The cytotoxicity experiment was performed three times (only twice for Ag@NO_2) with 3 technical replicates. Non-linear regression followed by an Absolute IC50 model was performed with baseline constant to 0 using GraphPad Prism version 9.0.0 for Windows, GraphPad Software, San Diego, California USA, http://www.graphpad.com.

Techniques

The morphology and size distribution of Ag NPs were investigated by TEM images, which were recorded by Tecnai microscope (120 kV) and 4k × 4k Eagle camera (Thermofisher, USA). All the carbon grids were primarily subjected to glow discharge treatment, followed by deposition of 4 μL of sample and incubation under room temperature for 1 min. Then 50 μL of uranyl acetate (2%) was added on the grids before TEM imaging. The extinction spectra of Ag NPs and stability of the colloidal solutions were studied by UV-vis spectroscopy (Shimadzu 2700 UV-vis spectrometer). The SERS spectra and Raman images of cells were recorded using a Horiba XploRA PLUS Raman microscope with 638 nm laser and 2 s exposition time. Hydrodynamic diameters (D_H) were determined by dynamic light scattering (DLS) using a Vasco-Flex particle size analyzer (Cordouan Technologies).

Results and discussion

The main steps for the functionalization of Ag NPs by aryl diazonium salts are illustrated in Fig. 1. Spherical silver NPs were first synthesized by citrate reduction of $AgNO_3$, resulting in

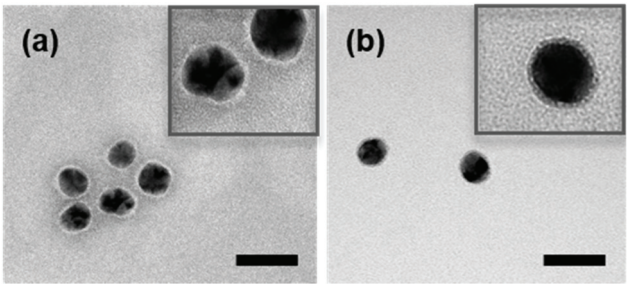

Fig. 2 Typical TEM images of (a) bare Ag NPs and (b) Ag@NO_2. Scale bare = 50 nm. The insets show zoom of each figure to better observe the surface coating.

NPs with an average diameter of *ca.* 25.9 nm (standard deviation σ_{TEM} = 4.9 nm), as observed by TEM (see Fig. 2 and Fig. S1†). The aryl diazonium salts (final concentration 5 μM) were then added to the aqueous Ag NPs colloidal solution ([Ag NPs] = 6.4 nM) and the reaction was carried out at room temperature during 60 min, after which 0.01 wt% polyvinylpyrrolidone (PVP) was added as a stabilizer. The obtained Ag NPs were purified through 3 cycles of centrifugation/redispersion in water, and named AgNP@R_1, where R_1 stands for the functional group carried by the first polyaryl layer.

For the bifunctional and trifunctional NPs, a second and third type of aryl diazonium salt (5 μM) were added after the first grafting step, using similar procedures as described above. The resulting SERS encoded tags were noted Ag@R_1@R_2@R_3, where R_{2-3} stands for the functional groups carried by the second and third polyaryl layers, respectively. The hydrodynamic diameters measured by DLS, before and after Ag NP functionalization, ranged from 32 to 51 nm (PDI between 0.24 and 0.31, see Table S1†). It is noteworthy that the functionalization steps do not modify the initial colloidal stability of Ag NPs, as observed from the TEM images recorded before and after reaction with diazonium salts, evidencing individually dispersed NPs (see Fig. 2 and Fig. S1†). The preservation of colloidal stability was also verified by recording the UV-vis spectra of the modified Ag NPs (see Fig. 3a and

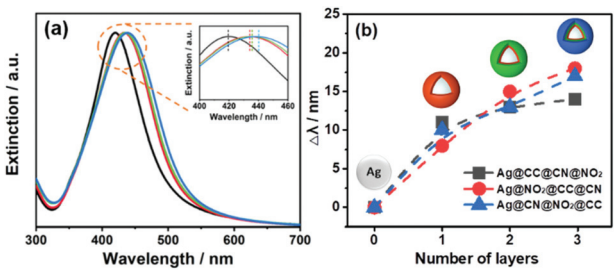

Fig. 3 (a) Normalized UV-vis spectra of Ag NPs (black line), Ag@CN (red line), Ag@CN@NO_2 (green line) and Ag@CN@NO_2@CCH (blue line); (b) Plot of $\Delta\lambda$ (red shift of plasmon band) *vs.* the number of grafted layers around Ag cores for the step-by-step functionalization of Ag@CCH@CN@NO_2, Ag@NO_2@CCH@CN and Ag@CN@NO_2@CCH.

Fig. S2†), revealing that the shape of the extinction curve was retained after functionalization.

In the meanwhile, the plasmon band progressively red shifted upon grafting of the polyaryl layers, with larger shifts (up to *ca.* 14–18 nm) observed in the presence of multifunctional layers (Fig. 3b). The colloidal stability of SERS labels was also assessed in concentrated NaCl solutions ($[NaCl]_{aq}$ = 0.2 M and 1 M). As observed in Fig. 4, the Ag NPs coated by single aryl layers (Ag@NO_2, Ag@CN, Ag@CCH) and PVP appear more stable than bare uncoated NPs, which immediately aggregate upon NaCl addition, even at the lowest tested concentration ([NaCl] = 0.2 M). However, the presence of single aryl layer coatings couldn't prevent NPs aggregation at high NaCl concentrations. Interestingly, the colloidal stability was further improved in the presence of multilayers, for which no sign of aggregation could be detected, even after the addition of high NaCl concentrations (1 M). The colloidal stability of all samples was also assessed over time in both pure water media or 0.2 M NaCl solutions. The shape of the extinction spectra remained unchanged after 7 weeks (see Fig. S3†) with no sign of aggregation, confirming the long-time stability of the SERS labels.

The SERS spectra displayed in Fig. 5 were recorded from dried drops of Ag NPs samples deposited on a glass plate, using a 638 nm laser source. It is noteworthy that the SERS spectra recorded on Ag NPs colloidal dispersions (Fig. S4†) were very similar to the ones obtained on dried drops but with lower signal intensities. For all samples, the spectra revealed the characteristic signatures of the polyaryl layers grafted around the Ag NP cores. The aryl ring stretching peak can be observed at *ca.* 1550–1625 cm^{-1} and the Ag–C stretching vibration appears at *ca.* 400 cm^{-1}, confirming the covalent nature of the interfacial bond between the silver surface and the aryl grafted layers.[42–44] In addition, each functional group brings distinct features, at 1325 cm^{-1} for NO_2 (ν_{NO_2}), 1960 cm^{-1} for CCH (ν_{CC}) and 2220 cm^{-1} for CN (ν_{CN}). It is to note that for all samples, the intense N≡N stretching vibration peak present in the Raman spectra of the parent aryl diazonium salts at *ca.* 2280–2300 cm^{-1} (Fig. S5†) is no more detectable after Ag NPs functionalization, in agreement with the release of N_2 upon grafting.[45] Interestingly, each combination of functional layers within the Ag NP coating leads to a different global SERS signature, which can be associated to a distinct code or color in Raman imaging. The formation of multilayers thus broadens the library of available Raman tags.

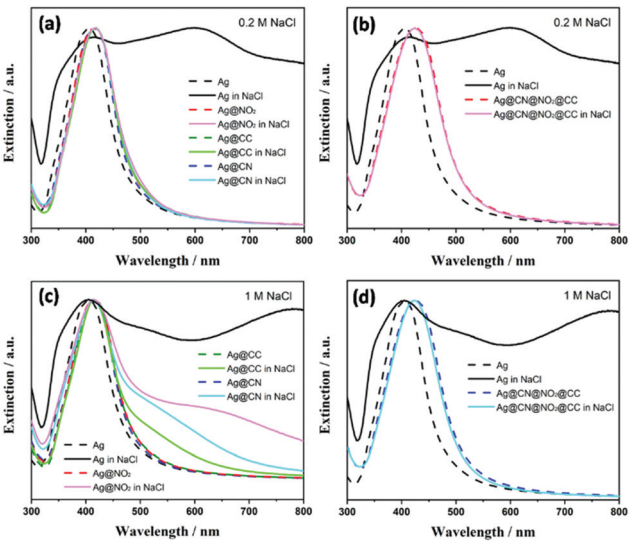

Fig. 4 Normalized UV-vis spectra of bare Ag NPs coated by (a and c) single polyaryl layers or (b and d) multilayers, before (dotted lines) and after (full line) addition of (a and b) NaCl (0.2 M) or (c and d) NaCl (1 M). It is noteworthy that 0.01 wt% PVP was present in all functionalized Ag NPs samples.

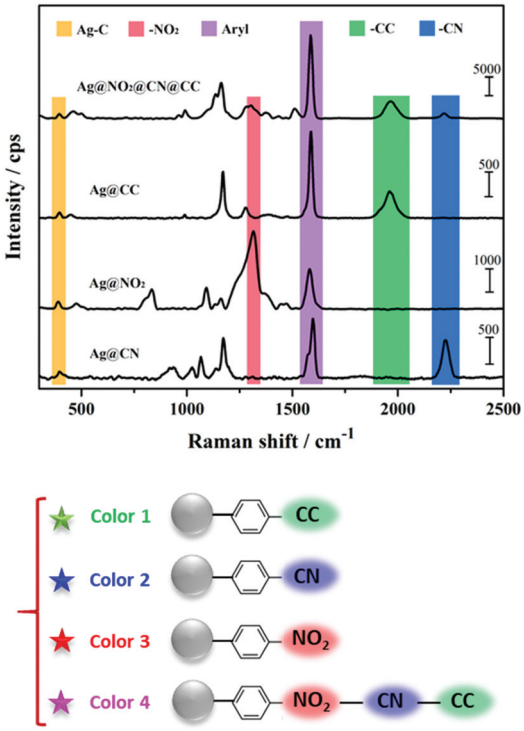

Fig. 5 SERS spectra of the three single layer-SERS tags and multilayer-coated Ag@NO_2@CN@CCH NPs. The excitation wavelength was 638 nm, and the exposure time was 2 s. The molecular structures of the three Raman reporters derived from aryl diazonium salts and the multilayer-coated Ag@NO_2@CN@CCH NPs are illustrated below.

Evaluation of the Raman labelling capacity of the functionalized Ag NPs for bioimaging was carried out by exposing HeLa-HSP70/GFP cells to the various SERS labels, re-suspended in 2 mL of medium to reach 20 μg mL^{-1}. Fig. 6 displays the Raman images of cells after NP uptake. The different NPs were incubated in individual cell cultures in 6 wells plates for 6 hours. Different colours were assigned to each characteristic signature: the signal of Ag@NO_2 was associated to the red, the Ag@CCH signal to the green and that of Ag@CN to the blue. The detection of the Raman reporter signals in localized area evidenced the presence of the NPs, probably accumulated within endosomal compartments. The multilayer-coated NPs offer additional vibrational fingerprints, based on the various

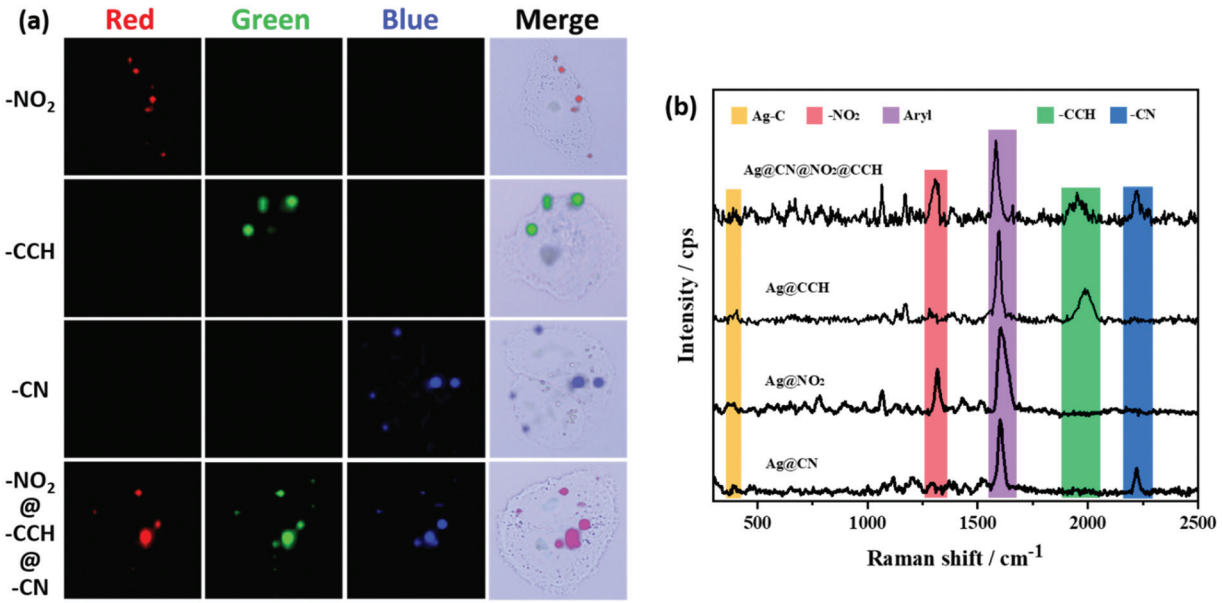

Fig. 6 (a) Raman images of HELA-HSP70/GFP cells after uptake of various SERS labels (re-suspended with 2 mL of medium to reach 20 μg mL^{-1}), as indicated on the left panel: Ag@NO_2, Ag@CCH, Ag@CN and Ag@CN@NO_2@CCH. The right column displays the overlay images of cell bright field pictures and Raman images. Scale bar: 5 μm. The Raman spectra in the red, green, and blue channels correspond to the signals of NO_2, CCH and CN, respectively. (b) Corresponding SERS spectra for each SERS tags. The SERS images were obtained with a 638 nm laser (30 mW) and a 100× objective lens.

possible combinations of peaks associated to the different functional groups present in the coating. For example, the signal of Ag@CN@NO_2@CCH NPs inside cells exhibits the characteristic peaks of each Raman labels (NO_2, CN, CCH), resulting in a distinct color code, here magenta. These results emphasize the great potential of diazonium salt chemistry to obtain a new generation of SERS labels based on Ag NPs for multiplex Raman bioimaging.

Cytotoxicity of SERS labels was assessed by an Alamar Blue assay. HeLa-HSP70/GFP cells were incubated with different amounts of SERS labels for 6 hours in 96-well plates. At the concentrations of NPs used for the Raman imaging experiments (20 μg mL^{-1}), the SERS labels exhibit cytotoxicity values (normalized viability) between 60 and 30% (Fig. 7 and Table S2† for raw data).

The cytotoxicity of SERS labels was also assessed on HeLa-HSP70/GFP in 6-well plates at 2 and 20 μg mL^{-1} (see Fig. S6 and Table S2,† Sheet Cytotoxicity in 6-well plate) and on fibroblasts (see Fig. S7 and Table S2†) showing similar values that the ones obtained with HeLa-HSP70/GFP in the 96-well plates. Interestingly, bare uncoated Ag NPs exhibit a slightly more cytotoxic effect, suggesting that surface functionalization by aryl diazonium salts tends to reduce cytotoxicity.

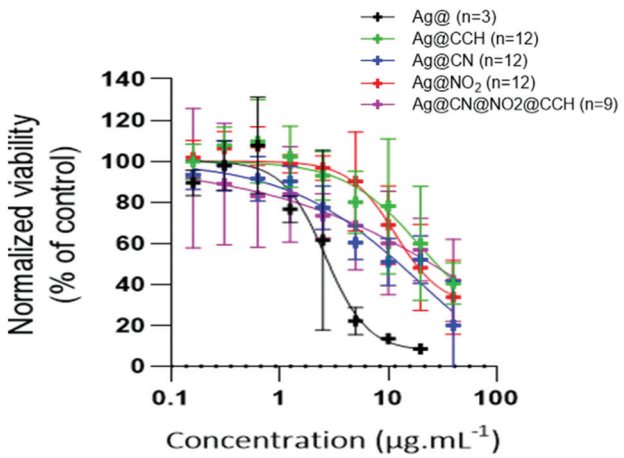

Fig. 7 Viability of HELA-HSP70/GFP cells after incubation with different amounts of SERS labels and bare uncoated Ag NPs, for 6 hours.

Conclusions

Aryl diazonium salt chemistry was used to functionalize Ag NPs for the design of a new generation of SERS encoded-nanoparticles. Ag NPs functionalized by multifunctional polyaryl layers bearing different Raman reporter groups (–NO_2, –CN, –CCH) were obtained using this approach. This surface functionalization strategy offers a promising alternative to thiol self-assembled monolayers, with the possibility to form multilayers around the silver cores, through a fast and user-friendly protocol (water solvent, air, room temperature). The surface polymerization of multiple Raman codes was shown to provide access to new spectral combinations thus broadening the library of available SERS tags. In addition, the presence of covalent bonds between the Raman labels and the silver cores guarantees the robustness of the SERS labels. After internaliz-

ation in HeLa-HSP70/GFP cell lines and likely accumulation in endosomes, the various SERS-encoded NPs could be visualized as distinct bright spots with spectrally distinguishable codes. These proof-of-concept results demonstrate the valuable assets of aryl diazonium salts to design Ag NPs-based SERS tags for Raman imaging.

Conflicts of interest

The authors declare no competing financial interests.

Acknowledgements

The authors thank Gérard Pehau-Arnaudet (Institut Pasteur) for the TEM analysis, Gregory Lavieu for providing the HELA-HSP70/GFP cells and Horiba for access to the Raman imaging facility. This work is supported in part by the scholarship from China Scholarship Council (CSC) under the Grant CSC No.201909370060. This study was supported by the IdEx Université de Paris, ANR-18-IDEX-0001 (plateforme IVETh and Emergence FLORIM) and by the Region Ile de France under the convention SESAME 2019 – IVETh (no. EX047011).

Notes and references

1 G. Q. Wallace and J.-F. Masson, *Analyst*, 2020, **145**, 7162–7185.
2 J. Yao, M. Yang and Y. Duan, *Chem. Rev.*, 2014, **114**, 6130–6178.
3 X. Han, K. Xu, O. Taratula and K. Farsad, *Nanoscale*, 2019, **11**, 799–819.
4 S. M. Mousavi, M. Zarei, S. A. Hashemi, S. Ramakrishna, W.-H. Chiang, C. W. Lai and A. Gholami, *Drug Metab. Rev.*, 2020, **52**, 299–318.
5 S. A. Maier, *Plasmonics: fundamentals and applications*, Springer Science & Business Media, 2007.
6 S. Lee, Y. Sun, Y. Cao and S. H. Kang, *Trends Anal. Chem.*, 2019, **117**, 58–68.
7 M. Nguyen, N. Felidj and C. Mangeney, *Chem. Mater.*, 2016, **28**, 3564–3577.
8 R. Ahmad, N. Félidj, L. Boubekeur-Lecaque, S. Lau-Truong, S. Gam-Derouich, P. Decorse, A. Lamouri and C. Mangeney, *Chem. Commun.*, 2015, **51**, 9678–9681.
9 J. Mosquera, Y. Zhao, H. J. Jang, N. Xie, C. Xu, N. A. Kotov and L. M. Liz-Marzán, *Adv. Funct. Mater.*, 2020, **30**, 1902082.
10 E. Lenzi, D. Jimenez de Aberasturi and L. M. Liz-Marzán, *ACS Sens.*, 2019, **4**, 1126–1137.
11 R. A. Alvarez-Puebla and L. M. Liz-Marzán, *Small*, 2010, **6**, 604–610.
12 Z. Wang, S. Zong, L. Wu, D. Zhu and Y. Cui, *Chem. Rev.*, 2017, **117**, 7910–7963.
13 M. Tabatabaei, D. McRae and F. Lagugné-Labarthet, Recent advances of plasmon-enhanced spectroscopy at bio-Interfaces, in *Frontiers of Plasmon Enhanced Spectroscopy*, ACS Publications, 2016, vol. 2, pp. 183–207.
14 A. Wokaun, J. Gordon and P. Liao, *Phys. Rev. Lett.*, 1982, **48**, 957.
15 M. A. Mahmoud and M. A. El-Sayed, *J. Phys. Chem. Lett.*, 2013, **4**, 1541–1545.
16 K. Kolwas and A. Derkachova, *Opto-Electron. Rev.*, 2010, **18**, 429–437.
17 C. Battocchio, C. Meneghini, I. Fratoddi, I. Venditti, M. V. Russo, G. Aquilanti, C. Maurizio, F. Bondino, R. Matassa and M. Rossi, *J. Phys. Chem. C*, 2012, **116**, 19571–19578.
18 B. Mir-Simon, I. Reche-Perez, L. Guerrini, N. Pazos-Perez and R. A. Alvarez-Puebla, *Chem. Mater.*, 2015, **27**, 950–958.
19 Y. Wang, B. Yan and L. Chen, *Chem. Rev.*, 2013, **113**, 1391–1428.
20 C. Hamon and L. M. Liz-Marzán, *J. Colloid Interface Sci.*, 2018, **512**, 834–843.
21 Q. Yu, Y. Wang, R. Mei, Y. Yin, J. You and L. Chen, *Anal. Chem.*, 2019, **91**, 5270–5277.
22 C. Vericat, M. Vela, G. Benitez, P. Carro and R. Salvarezza, *Chem. Soc. Rev.*, 2010, **39**, 1805–1834.
23 J. Walia, J.-M. Guay, O. Krupin, F. Variola, P. Berini and A. Weck, *Phys. Chem. Chem. Phys.*, 2018, **20**, 238–246.
24 X. Zhuo, M. Henriksen-Lacey, D. J. Aberasturi, A. Sánchez-Iglesias and L. M. Liz-Marzán, *Chem. Mater.*, 2020, **32**, 5879–5889.
25 D. Hetemi, V. Noël and J. Pinson, *Biosensors*, 2020, **10**, 4.
26 A. Berisha, C. Combellas, F. d. r. Kanoufi, P. Decorse, N. Oturan, J. r. m. Médard, M. Seydou, F. o. Maurel and J. Pinson, *Langmuir*, 2017, **33**, 8730–8738.
27 M. Bouriga, M. M. Chehimi, C. Combellas, P. Decorse, F. d. r. Kanoufi, A. Deronzier and J. Pinson, *Chem. Mater.*, 2013, **25**, 90–97.
28 M. Nguyen, I. Kherbouche, S. Gam-Derouich, I. Ragheb, S. Lau-Truong, A. Lamouri, G. Lévi, J. Aubard, P. Decorse and N. Félidj, *Chem. Commun.*, 2017, **53**, 11364–11367.
29 M. Nguyen, A. Lamouri, C. Salameh, G. Lévi, J. Grand, L. Boubekeur-Lecaque, C. Mangeney and N. Félidj, *Nanoscale*, 2016, **8**, 8633–8640.
30 J. Pinson and F. Podvorica, *Chem. Soc. Rev.*, 2005, **34**, 429–439.
31 Y. Zhao, L. Tong, Z. Li, N. Yang, H. Fu, L. Wu, H. Cui, W. Zhou, J. Wang and H. Wang, *Chem. Mater.*, 2017, **29**, 7131–7139.
32 C. Cao, Y. Zhang, C. Jiang, M. Qi and G. Liu, *ACS Appl. Mater. Interfaces*, 2017, **9**, 5031–5049.
33 Z. Chen, Y. Xie, W. Huang, C. Qin, A. Yu and G. Lai, *Nanoscale*, 2019, **11**, 11262–11269.
34 Y. Kalachyova, A. Olshtrem, O. A. Guselnikova, P. S. Postnikov, R. Elashnikov, P. Ulbrich, S. Rimpelova, V. Švorčík and O. Lyutakov, *ChemistryOpen*, 2017, **6**, 254–260.
35 Y. Luo, Y. Xiao, D. Onidas, L. Iannazzo, M. Ethève-Quelquejeu, A. Lamouri, N. Félidj, S. Mahouche-Chergui,

T. Brulé and N. Gagey-Eilstein, *Chem. Commun.*, 2020, **56**, 6822–6825.
36 T. Dai, N. Li, F. Han, H. Zhang, Y. Zhang and Q. Liu, *Biomaterials*, 2016, **83**, 37–50.
37 V. Q. Nguyen, Y. Ai, P. Martin and J. C. Lacroix, *ACS Omega*, 2017, **2**, 1947–1955.
38 D. A. B. Therien, D. M. McRae, C. Mangeney, N. Félidj and F. Lagugné-Labarthet, *Nanoscale Adv.*, 2021, **3**, 2501–2507.
39 Y. Zeng, K. M. Koo, M. Trau, A. G. Shen and J. M. Hua, *Appl. Mater. Today*, 2019, **15**, 431–444.
40 L. A. Austin, B. Kang, C.-W. Yen and M. A. El-Sayed, *J. Am. Chem. Soc.*, 2011, **133**, 17594–17597.
41 B. Emeline and G. Lavieu, *FEBS Lett.*, 2019, **593**, 1983–1992.
42 L. Laurentius, S. R. Stoyanov, S. Gusarov, A. Kovalenko, R. Du, G. P. Lopinski and M. T. McDermott, *ACS Nano*, 2011, **5**, 4219–4227.
43 F. Mirkhalaf, J. Paprotny and D. J. Schiffrin, *J. Am. Chem. Soc.*, 2006, **128**, 7400–7401.
44 L. Troian-Gautier, H. Valkenier, A. Mattiuzzi, I. Jabin, N. Van den Brande, B. Van Mele, J. Hubert, F. Reniers, G. Bruylants and C. Lagrost, *Chem. Commun.*, 2016, **52**, 10493–10496.
45 M. Supur, S. R. Smith and R. L. McCreery, *Anal. Chem.*, 2017, **89**, 6463–6471.